



Heterogeneous & Homogeneous & Bio- & Nano-

CHEM **CAT** CHEM

CATALYSIS

Accepted Article

Title: Formic Acid Decomposition over ZnPd - Implications for Methanol Steam Reforming

Authors: René Kriegel, Dennis Ivarsson, and Marc Armbrüster

This manuscript has been accepted after peer review and appears as an Accepted Article online prior to editing, proofing, and formal publication of the final Version of Record (VoR). This work is currently citable by using the Digital Object Identifier (DOI) given below. The VoR will be published online in Early View as soon as possible and may be different to this Accepted Article as a result of editing. Readers should obtain the VoR from the journal website shown below when it is published to ensure accuracy of information. The authors are responsible for the content of this Accepted Article.

To be cited as: *ChemCatChem* 10.1002/cctc.201800194

Link to VoR: <http://dx.doi.org/10.1002/cctc.201800194>

WILEY-VCH

www.chemcatchem.org



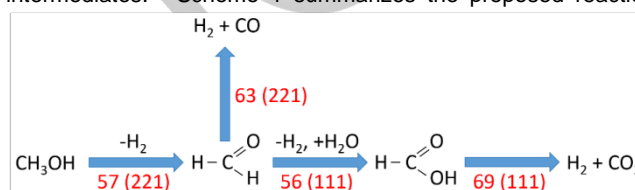
Formic Acid Decomposition over ZnPd – Implications for Methanol Steam Reforming

René Kriegel,^[a] Dennis C. A. Ivarsson,^[a] and Marc Armbrüster^{*[a]}

Abstract: Single-phase ZnPd with different elemental composition as well as ZnO-supported ZnPd nanoparticles were prepared and tested concerning their catalytic properties in the formic acid decomposition with the aim to investigate a possible formate pathway in the steam reforming of methanol (MSR). Pd-rich ZnPd showed higher catalytic activity in comparison to ZnPd with lower Pd-content. All samples showed high and stable CO₂-selectivity. The stability of the materials was investigated both *ex situ* by powder X-ray diffraction (XRD), scanning electron microscopy (SEM) and Raman spectroscopy after formic acid decomposition as well as by *in situ* X-ray photoelectron spectroscopy (*in situ* XPS) and *operando* DTA/TG and resulted in higher stability against oxidation for samples with higher Pd-content, corroborating earlier observations under MSR conditions. The supported ZnPd/ZnO material and Zn-rich bulk ZnPd samples showed a strong modification after reaction, which is attributed to zinc formate formation during formic acid decomposition. Kinetic data give strong indications to exclude dehydrogenation of a formate intermediate as rate limiting step in MSR.

chemical potential (in particular when starting from equimolar chemical composition).^[7] While these studies shed light on the material changes under reaction conditions, the reaction mechanism of methanol steam reforming is far from being completely understood.

To increase the knowledge on the MSR reaction mechanism, numerous quantum chemical calculations on the catalytic properties of ZnPd were conducted regarding possible intermediates.^[8] Scheme 1 summarizes the proposed reaction



sequence on different ZnPd surfaces, indicating formaldehyde as a key intermediate in MSR.

Scheme 1. Proposed reaction pathways for MSR on different ZnPd surfaces based on quantum chemical calculations. The lowest activation energies in kJ mol⁻¹ and the involved surfaces for the reaction steps are given in red.^[8b, 8d, 8f]

Introduction

Methanol is a promising molecule to serve as hydrogen carrier.^[1] Via methanol steam reforming (MSR, CH₃OH + H₂O → 3 H₂ + CO₂) the chemically stored hydrogen can be easily released on demand for usage in fuel cell applications.^[2] Here, the production of high purity hydrogen, i.e. avoiding CO contamination is crucial, since for a long-term stable performance of proton exchange membrane fuel cells (PEMFCs) CO concentrations should not exceed 10 ppm.^[3]

The intermetallic compound ZnPd has been shown to be a promising catalytic material for MSR because of its high CO₂-selectivity of up to 99.4% and thermal stability.^[4] Studies on unsupported ZnPd revealed that the coexistence of ZnPd and ZnO is necessary for the high CO₂-selectivity,^[5] whereas single-phase ZnPd preferentially catalyzes methanol decomposition.^[6] The high CO₂-selectivity of unsupported ZnPd results from the formation of an oxidized Zn-species under MSR conditions, which leads to the highly selective ZnPd/ZnO interface.^[6] The strong compositional dependence of the catalytic properties results from the change in chemical potential with the chemical composition of ZnPd. In this respect, even a small change in the chemical composition of ZnPd can result in a significant change of the

C-H splitting of the formaldehyde intermediate results in unwanted methanol decomposition and therefore in CO formation. The dehydrogenation of formaldehyde is kinetically unfavorable on ZnPd surfaces, unless water activation for MSR is not hindered sufficient enough.^[8b] Experiments as well as quantum chemical calculations provide indications for improved water activation by the presence of ZnO.^[6, 9] This circumstance explains the increasing CO₂-selectivity by presence of ZnO, e.g. on partially oxidized ZnPd surfaces.^[5]

To optimize future catalytic materials, the question concerning the rate limiting step (RLS) in MSR has been addressed by DFT calculations taking into account the presence of methanol and water simultaneously on ZnPd(111). The calculated activation energy of 86 kJ mol⁻¹ for the formaldehyde formation as RLS^[8d] is significantly higher than the experimental apparent activation energy, reported to be 69 kJ mol⁻¹.^[6] This implies that the calculations on ZnPd(111) do not result in an overall picture of the underlying mechanism. Considering also other investigated surfaces, the abstraction of the last hydrogen from a formate intermediate becomes a likely candidate for the rate limiting step with an activation energy of 69 kJ mol⁻¹.^[10] This assumption gets encouraged by experimental studies assigning the formate species as key surface intermediate.^[11]

Formic acid decomposition presents a suitable model reaction to investigate a small part of the likely MSR reaction mechanism. Formic acid, as precursor for formate, represents a test molecule, where the MSR reagents methanol and water are already combined. In addition, formic acid decomposition represents a

[a] M. Sc. R. Kriegel, M. Sc. D.C.A. Ivarsson, Prof. Dr. M. Armbrüster
Institute of Chemistry
Technische Universität Chemnitz
Straße der Nationen 62, 09111 Chemnitz (Germany)
E-mail: marc.armbruester@chemie.tu-chemnitz.de

Supporting information for this article is given via a link at the end of the document.

FULL PAPER

common used model reaction to study the catalytic activity of metals and alloys^[12] as well as intermetallic compounds,^[13] thus enabling further understanding of ZnPd by comparison. Lorenz et al. investigated the decomposition of formic acid on intermetallic GaPd₂/β-Ga₂O₃ and single-phase β-Ga₂O₃.^[14] Comparing the results to the data from MSR tests on the same material, they assumed that the dehydrogenation of a formate species represents the last step in MSR mechanism. Furthermore, they supposed that the dehydrogenation preferably takes place on the intermetallic compound. Jeroro and Vohs studied the decomposition of formic acid on Zn/Pd(111) surface alloys under ultra-high vacuum (UHV) conditions.^[15] Using temperature-programmed desorption (TPD) and high-resolution electron energy loss spectroscopy they were able to detect the formation of a formate intermediate on the surface. This observation affirms the usability of formic acid for investigations of formate dehydrogenation.

The aim of the present work is to enlarge the understanding of MSR on intermetallic compounds. Therefore, unsupported single-phase ZnPd as well as ZnO-supported ZnPd particles were prepared and tested in the formic acid decomposition in a plug-flow reactor. Owing to the different catalytic behavior of ZnPd with chemical composition,^[6] three samples of bulk Zn_{100-x}Pd_x ($x = 48.1-58.0$) were tested. Before the catalytic measurements, bulk characterization by powder X-ray diffraction (XRD) and ICP-OES was carried out. SEM and XRD were applied to investigate the samples additionally after formic acid decomposition. Activity, selectivity and apparent activation energy were determined for the three samples.

Results and Discussion

Synthesis and Characterization

According to the latest phase diagram the intermetallic compound ZnPd exists between 47 and 62.5 at.-% Pd at 900 °C.^[10] Thus the nominally compositions of the samples were chosen as 48.1 at.-%, 50.1 at.-% and 58.0 at.-% Pd to allow for the formation of single-phase ZnPd. No phase besides ZnPd could be detected by XRD (Figure S1). The observed shift of the reflections results from the different compositions of the samples, which in turn results in a change of the lattice parameters.^[6] ICP-OES analysis yielded Pd-contents of 46.7(2) at.-%, 49.1(1) at.-% and 57.1(2) at.-% for the respective ZnPd samples. Since chemical analyses and expected chemical compositions differed slightly, compositions were also determined by weighing the samples before and after synthesis. Because no reaction with the ampoule material was observed, the difference between the initial and the end mass should clarify if all provided Zn reacted with Pd during synthesis. By weighing the nominal compositions of bulk ZnPd samples could be confirmed (48.1 at.-%, 50.2 at.-% and 58.0 at.-% Pd and a standard deviation of less than 0.01 at.-%). Therefore, hereafter the chemical composition determined by weighing will be used.

The pre-calcined PdO/ZnO was used as precursor to prepare ZnO-supported ZnPd particles by reactive metal-support interaction (RMSI).^[16] The precursor system was directly reduced

in hydrogen at 200 °C for 1 h to first reduce palladium oxide to palladium and subsequently partly reduce the ZnO in the vicinity of the palladium particles to elemental zinc. This then diffuses into the palladium and forms the intermetallic compound ZnPd. As expected, the obtained X-ray diffraction pattern results in the observation of ZnPd, ZnO and Pd (Figure S2). The latter is only observed as trace – consistent with earlier publication – and is expected to be encapsulated in ZnO, according to high resolution transmission electron microscopy (HRTEM).^[5] Thus Pd should not contribute to the catalytic properties. The lower Pd-loading of the supported sample, determined by ICP/OES to be 7.8(3) at.-% compared to the nominal loading of 9.7 at.-%, is likely due to the unknown amount of water in the used Pd(NO₃)₂ · xH₂O.

Catalysis and ex situ Characterization of Bulk ZnPd

To achieve direct comparability of the catalytic formic acid decomposition on ZnPd with different chemical compositions, the tests were conducted with identical reaction parameters and identical masses of 50 mg. Figure 1 summarizes the obtained conversion and CO₂-selectivity of the bulk ZnPd samples as a function of temperature.

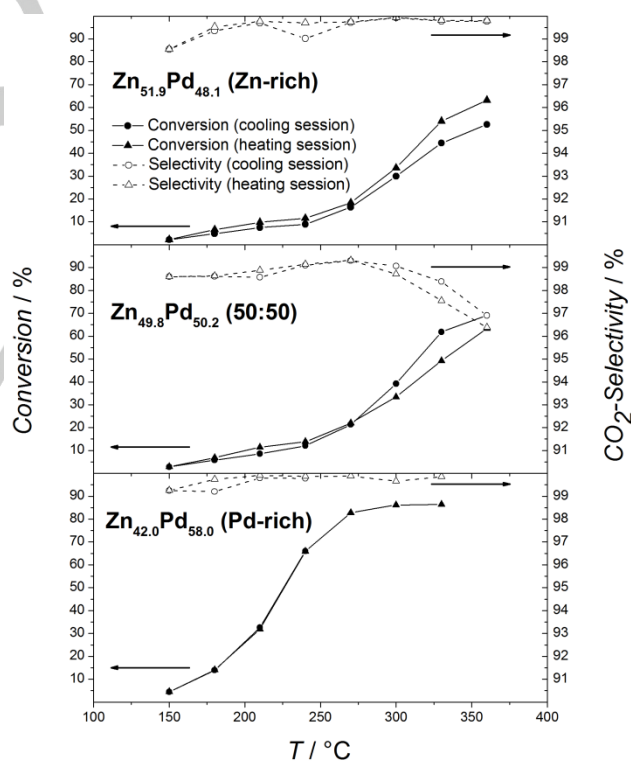


Figure 1. Conversion and CO₂-Selectivity of bulk Zn_{100-x}Pd_x (50 mg) in formic acid decomposition. Lines are a guide to the eyes.

An obvious activity difference between the Pd-rich ZnPd and the samples with lower Pd-content can be observed. For a quantitative comparison the activities at 270 °C are considered in the following. Zn_{51.9}Pd_{48.1} ($A = 21 \text{ mmol}_{\text{COX}} \text{ mmol}_{\text{Pd}}^{-1} \text{ h}^{-1}$) and

FULL PAPER

$\text{Zn}_{49.8}\text{Pd}_{50.2}$ ($A = 25 \text{ mmol}_{\text{CO}_x} \text{ mmol}_{\text{Pd}}^{-1} \text{ h}^{-1}$) differ only by 19% in activity ($\text{Zn}_{49.8}\text{Pd}_{50.2} > \text{Zn}_{51.9}\text{Pd}_{48.1}$), whereas $\text{Zn}_{42.0}\text{Pd}_{58.0}$ exhibited a value roughly 4-times higher ($A = 85 \text{ mmol}_{\text{CO}_x} \text{ mmol}_{\text{Pd}}^{-1} \text{ h}^{-1}$). This difference in the catalytic properties of the chemically differently composed ZnPd samples is also displayed in the selectivity towards CO_2 . While $\text{Zn}_{51.9}\text{Pd}_{48.1}$ and $\text{Zn}_{42.0}\text{Pd}_{58.0}$ show no significant temperature dependence of the CO_2 -selectivity (98.5-99.9% and 99.5-99.9%, respectively), $\text{Zn}_{49.8}\text{Pd}_{50.2}$ reveals a reversible decrease of the CO_2 -selectivity (down to 96%) with increasing reaction temperature.

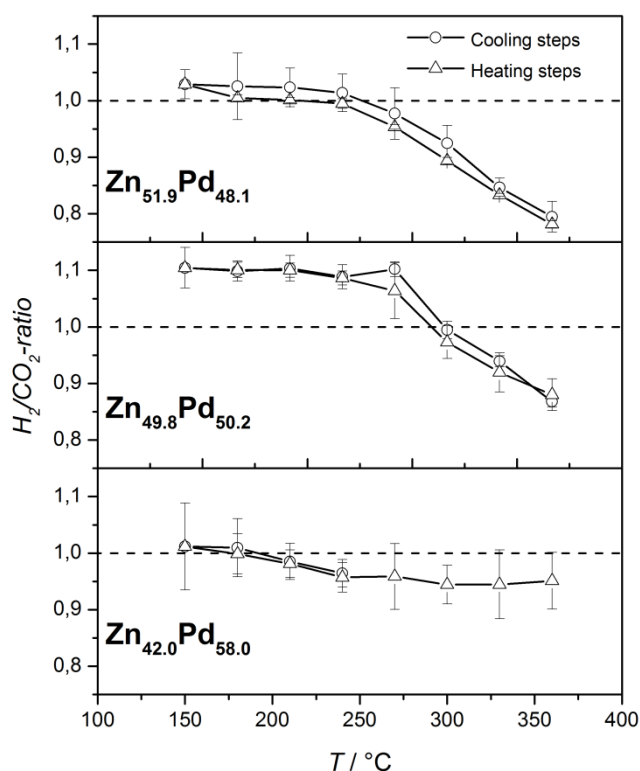


Figure 2. H_2/CO_2 -ratio of bulk ZnPd in formic acid decomposition. Lines are a guide to the eyes.

In Figure 2 the ratio between H_2 and CO_2 in the product gas as function of reaction temperature is depicted. If only dehydrogenation and/or dehydration of formic acid proceed, this ratio should be one. Therefore, this value provides information about additionally ongoing other processes.

For all samples the H_2/CO_2 -ratio was initially 1.0 within the standard deviation. With increasing temperature the ratio started to decrease. Above 240 °C $\text{Zn}_{51.9}\text{Pd}_{48.1}$ and $\text{Zn}_{49.8}\text{Pd}_{50.2}$ showed a drastic drop with a minimum value of around 0.8 and 0.9, respectively. The drop of the H_2/CO_2 -ratio was reversible during cooling and the second heating. However, the palladium-rich sample $\text{Zn}_{42.0}\text{Pd}_{58.0}$ did not share such a drop of the H_2/CO_2 -ratio and reached a constant value of about 1.0. Thus, the significant change of the H_2/CO_2 -ratio for $\text{Zn}_{51.9}\text{Pd}_{48.1}$ and $\text{Zn}_{49.8}\text{Pd}_{50.2}$ is connected to a reversible change of the samples during formic

acid decomposition. This alteration must involve consumption of hydrogen.

X-ray diffraction patterns of the catalyst samples after formic acid decomposition (Figure 3) were recorded to investigate the changes appearing under reaction conditions. For this purpose, the catalyst samples were cooled down to room temperature in inert atmosphere (N_2 , 60 mL min^{-1}) after finishing the (second) heating step and were directly analyzed afterwards. The patterns were compared to the measured diffraction pattern of the filling material graphite, as well as to calculated patterns of ZnPd and ZnO. At a first view only the reflections of graphite and ZnPd can be observed. By magnification of the patterns in the range between 30 and 40 ° also the main peaks of ZnO become visible in the patterns of $\text{Zn}_{49.8}\text{Pd}_{50.2}$ and $\text{Zn}_{51.9}\text{Pd}_{48.1}$, while for the sample $\text{Zn}_{42.0}\text{Pd}_{58.0}$ no signal is observed in this region.

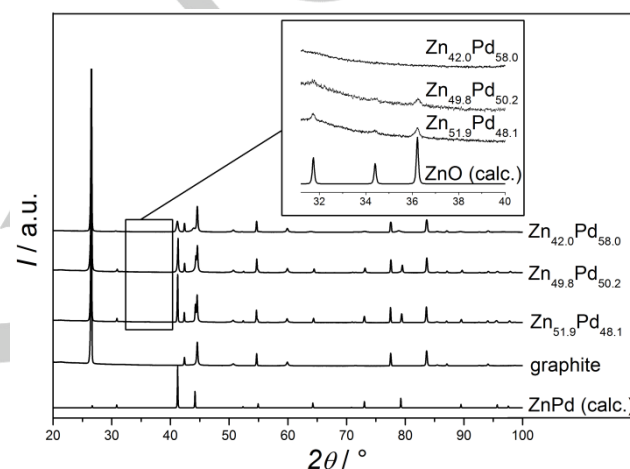


Figure 3. X-ray diffraction patterns of bulk $\text{Zn}_{100-x}\text{Pd}_x$ after formic acid decomposition.

Friedrich et al. have shown that ZnO is formed on the surface of $\text{Zn}_{51.9}\text{Pd}_{48.1}$ under MSR conditions.^[6] The authors attribute the high activity of ZnPd in MSR to this phenomenon. In contrast, for Pd-rich ZnPd stronger resistance in surface oxidation was observed, which resulted in lower MSR activity. Here, it is assumed that $\text{Zn}_{51.9}\text{Pd}_{48.1}$ and $\text{Zn}_{49.8}\text{Pd}_{50.2}$ samples pass an oxidation/reduction during the heating/cooling in formic acid, which results in a change of the H_2/CO_2 ratio as well as of the catalytic properties. At low temperatures ($\leq 240 \text{ °C}$) the reaction atmosphere possesses a more oxidative character due to the lower conversion and thus a lower hydrogen content. This leads to the oxidation of the Zn-rich samples and the formation of ZnO as observed by *ex situ* XRD. The partial coverage of the metal surface with oxidized species seems to have a negative influence of the catalytic activity as was already seen for $\text{GaPd}_2/\beta\text{-Ga}_2\text{O}_3$.^[14] The generated ZnO further reacts with formic acid to zinc formate as shown by Noto et al. using *in situ* infrared spectroscopy during formic acid decomposition on pure ZnO.^[17] Higher temperatures ($> 250 \text{ °C}$) cause the decomposition of zinc formate under formation of ZnO, hydrogen, carbon monoxide and carbon dioxide as main products whereas hydrogen and carbon

FULL PAPER

monoxide are able to form formaldehyde in a second reaction step.^[18] If only decomposition of zinc formate above 240 °C would influence the H₂/CO₂ ratio one would expect a short decrease of the values followed by an equalization with time. Because of the fact that the H₂/CO₂ ratio is rather temperature- than time-dependent (decreasing H₂/CO₂ ratio with increasing temperature), there has to be a second reason for the unusual behavior. An emerging side reaction could be an explanation. Conceivable side reactions as water gas shift reaction and formaldehyde formation by hydrogenation of CO can be excluded because the first one would not alter the H₂/CO₂ ratio and formation of formaldehyde out of syngas is reported as not being feasible.^[19] Methanol synthesis from CO₂, reported by Iwasa et al. at ambient pressure over ZnPd supported on ZnO,^[20] could explain the observed decrease of the H₂/CO₂ ratio. The necessary simultaneous presence of ZnPd and ZnO is in our case only achieved for the samples Zn_{49.8}Pd_{50.2} and Zn_{51.9}Pd_{48.1} above 240 °C. In contrast, Zn_{42.0}Pd_{58.0} is more resistant against oxidation and therefore, the methanol synthesis is not feasible. Thus, methanol synthesis explains the observed catalytic properties as well as the behavior of the H₂/CO₂-ratio.

Catalytic Properties of ZnO-Supported ZnPd

For the formic acid decomposition on the supported catalyst ZnPd/ZnO identical reaction conditions as for bulk ZnPd were applied. Because of the higher activity of the supported material, a lower sample mass of 10 mg was used. Figure 4 shows the conversion and CO₂-selectivity of the supported sample. A strong difference in activity between the first and second heating is observed (not shown). During the first heating up to 240 °C ZnPd/ZnO shows lower conversion in comparison with the second heating session. Between 240 and 270 °C – the assigned region for zinc formate decomposition – conversion and selectivity of the first and second heating suddenly assimilate. In difference to the unsupported samples, ZnPd/ZnO was not crushed before the catalytic tests. Therefore, the difference between the first and second heating cannot be explained by healing of surface irregularities caused by mechanical stress.

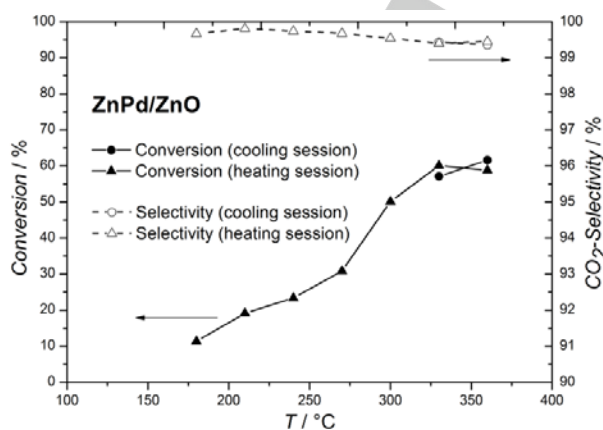


Figure 4. Conversion and CO₂-selectivity of ZnPd/ZnO (10 mg) in formic acid decomposition. Lines are a guide to the eyes.

The obtained activity (1268 mmol_{CO_x} mmol_{Pd}⁻¹ h⁻¹ at 270 °C) was much higher than for the tested bulk ZnPd. The observed CO₂-selectivity was stable and as high as for the bulk samples (99.2-99.8%). A view of the H₂/CO₂-ratio during formic acid decomposition (Figure 5) shows a characteristic, which is similar to Zn_{49.8}Pd_{50.2} and Zn_{51.9}Pd_{48.1} regarding the temperature where the ratio changes strongly (240 °C). The second heating of the catalyst showed that this phenomenon is reproducible and reversible.

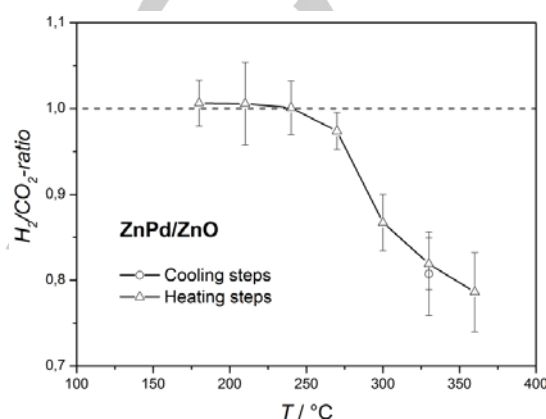


Figure 5. H₂/CO₂-ratio of ZnPd/ZnO in formic acid decomposition. Lines are a guide to the eyes.

To check for material changes during catalysis, X-ray diffraction patterns after formic acid decomposition were recorded (Figure 6). For this purpose, the catalyst sample was cooled down to room temperature in inert atmosphere (N₂, 60 mL min⁻¹) after finishing the (second) heating step and was directly analyzed afterwards. The pattern showed the expected peaks of ZnPd and the support, while the prior observed Pd-reflections are no longer detectable. Furthermore, the relative intensity of the ZnO reflections is much lower in comparison to the pattern of the material after reduction.

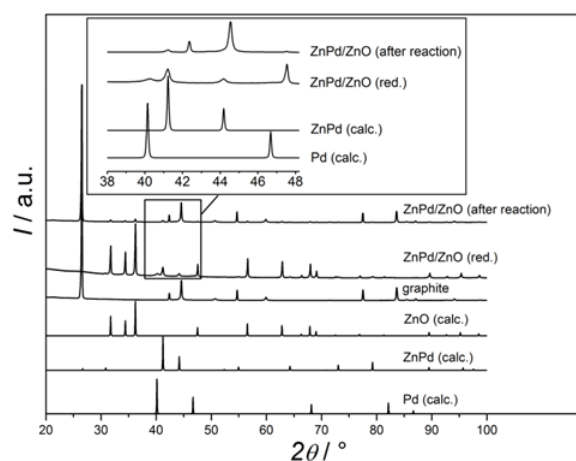


Figure 6. X-ray powder diffraction patterns of ZnPd/ZnO after pretreatment and after formic acid decomposition. The inner window shows a magnification of the

FULL PAPER

X-ray powder diffraction patterns (the signals at 42.5 ° and 47.5 ° belong to graphite and ZnO, respectively).

The discrepancies can either be explained by a significant leaching of Zn during reaction or by a strong Zn-enrichment of the intermetallic ZnPd. Analysis of the Zn/Pd mass ratio from the catalyst sample before – Pd: 8.8(4) wt.-% / Zn: 63.9(8) wt.-% – and after – Pd: 0.23(1) wt.-% / Zn: 1.26(2) wt.-% - formic acid decomposition determined by ICP-OES was conducted to reassess possible leaching. The smaller mass percent of Pd and Zn after reaction are explained by the dilution of the catalyst sample through the inert filling material. After normalizing to 100, the Zn/Pd ratios before – Pd: 12.1(5) wt.-% / Zn: 88(1) wt.-% – and after – Pd: 15.4(7) wt.-% / Zn: 85(1) wt.-% - formic acid decomposition showed a slight Zn decrease after reaction, not explaining the observations by XRD after reaction. The lattice parameters of the supported ZnPd before ($a = 2.8962(1) \text{ \AA}$, $b = 3.3402(3) \text{ \AA}$) and after ($a = 2.8979(3) \text{ \AA}$, $b = 3.3405(6) \text{ \AA}$) reaction do not show a large deviation, thus excluding a vast zinc-enrichment of the ZnPd. Since no additional Zn-species can be detected by XRD but the total zinc content stays constant, some of the zinc must be present in amorphous form.

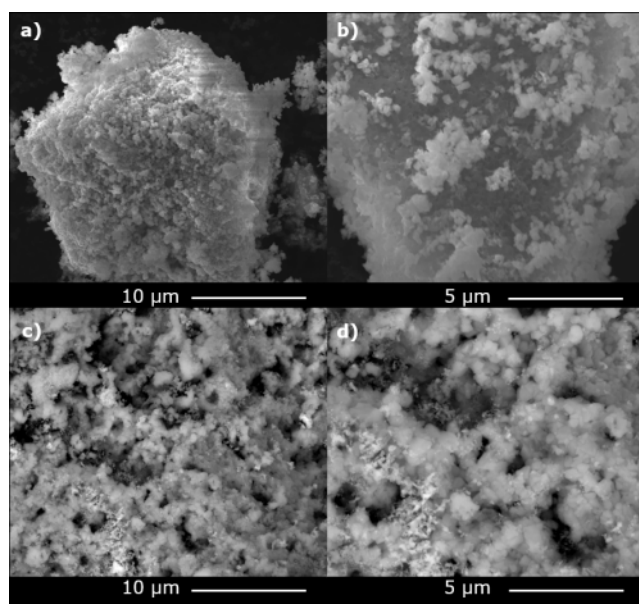


Figure 7. SEM images (BSE micrographs) of ZnPd/ZnO before (a, b) and after (c, d) formic acid decomposition.

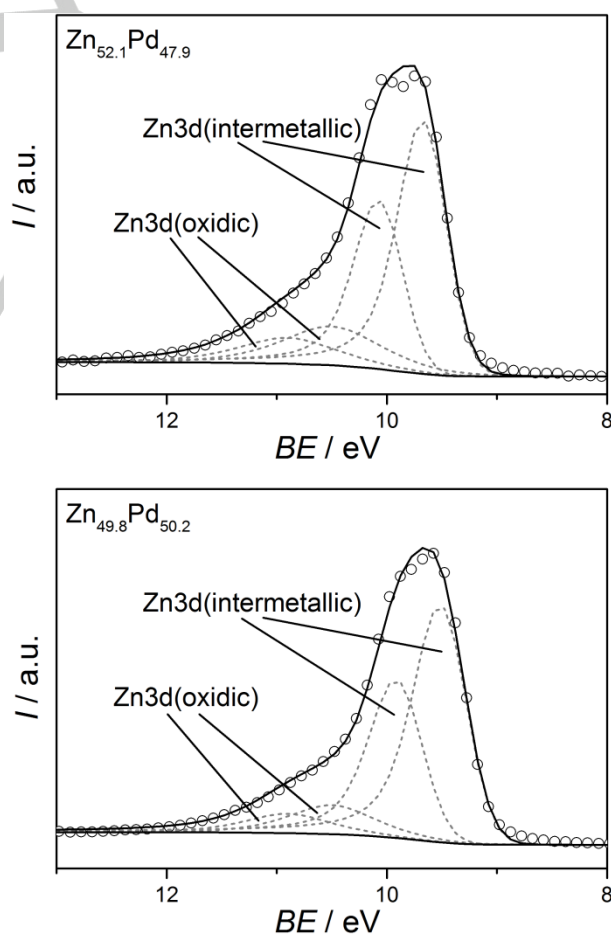
SEM investigations show strong differences between ZnPd/ZnO directly after reduction and the catalyst sample after reaction (Figure 7). The morphology of the support has drastically changed due to the formic acid decomposition. After reaction, the ZnO support shows fine pores and possesses a less compact morphology.

Most likely, the reason for the different relative reflection intensities (shown in Figure 6) lies in the change of the crystallinity

of the ZnO during reaction. As shown above, ZnO can form zinc formate under formic acid decomposition conditions. The transformation of ZnO into zinc formate and backwards apparently results in lower crystallinity. This dynamic behavior might also well be the reason for the disappearance of the Pd reflections. Here, the originally encapsulated elemental Pd was transformed to ZnPd.

Reactivity

XPS measurements were conducted to affirm the different behavior with changing chemical composition and to explore the predominant states of the near-surface region before, during and after catalysis. Since in the supported material the presence of large amounts of ZnO can hinder the detection of changes, the bulk $\text{Zn}_{100-x}\text{Pd}_x$ ($x = 48.1\text{--}58.0$) samples were investigated after pre-reduction, *operando* during formic acid decomposition as well as after subsequent reduction. After pre-reduction signals with low intensity of $\text{Au}4d_{5/2}$ at 335.4 eV and $\text{Au}4p_{3/2}$ at 546.2 eV binding energy (BE) are detectable in the regions scans of Pd3d and Pd3p, respectively. The Au signals were too small to detect them beforehand in the survey measurement and are most likely a contamination from the XPS chamber.



FULL PAPER

Figure 8. XP spectra of the Zn3d region measured at $Zn_{52.1}Pd_{47.9}$ and $Zn_{49.8}Pd_{50.2}$ in the pre-reduced state. The spectra correspond to a photon energy of 237 eV.

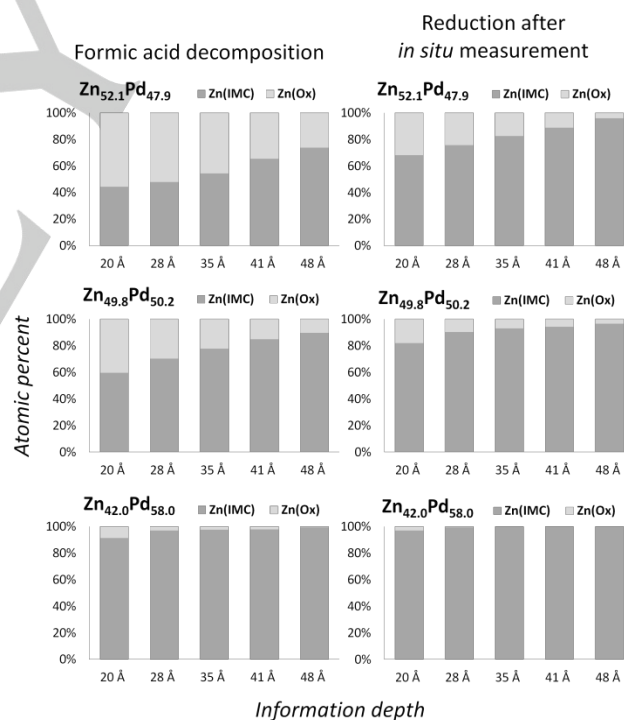
By evaluating the Zn3d region of the $Zn_{52.1}Pd_{47.9}$ and $Zn_{49.8}Pd_{50.2}$ sample two different Zn species with characteristic spin orbit coupling could be identified (Figure 8). The BE of the corresponding Zn3d_{5/2} signals were determined to be at 10.5 eV and 9.65 or 9.49 eV, respectively. While the quantity of the Zn species at higher BE was decreasing with increasing information depth, an inverse behavior was observed for the Zn species at lower BE (Figure S3). In the case of Pd-rich $Zn_{42.0}Pd_{58.0}$ only one signal at 9.30 eV appeared.

The signal at 10.5 eV in the samples can be assigned to a layer of an oxidized Zn-species, which is in line with the observed change in depth. According to that, the shifting signal with chemical composition can be described as Zn in the intermetallic compound ZnPd. The determined peak positions assort with former XPS investigations on ZnPd by Friedrich et al. where the oxidized Zn was also assumed to originate from the presence of zinc oxide.^[6] The shift of the intermetallic Zn3d signal with different chemical compositions is an indication for changes in the electronic state of the observed species within the samples and is also seen for the intermetallic Pd3d signals (Figure S4). While Friedrich et al. observed this compositional shift in their depth profiles due to zinc enrichment on the surface caused by mechanical stress, the newly developed synthesis protocol can circumvent this effect. The homogeneity of the bulk ZnPd samples could also be confirmed by calculating the Zn:Pd atomic ratios based on the fitted peak areas of the Zn3d and Pd3d signals. The ratios show no dependence with depth, ruling out segregation. Like in the study by Friedrich et al., the ZnPd samples show different oxidative behavior in such a way that $Zn_{52.1}Pd_{47.9}$ and $Zn_{49.8}Pd_{50.2}$ are not fully reducible at 200 °C in contrast to Pd-rich $Zn_{42.0}Pd_{58.0}$.

After UHV XPS investigations, 0.2 mbar formic acid were applied in the chamber while heating the samples to 200 °C. Once pressure and temperature were stabilized, complete depth profiles (Pd3d, Pd3p, Zn3d, O1s, C1s) under *operando* conditions were recorded. After formic acid decomposition, the ZnPd samples were reduced in 0.5 mbar hydrogen at 200 °C and full depth profiles were recorded in UHV ($\approx 10^{-8}$ mbar) at room temperature. Figure 9 displays the atomic Zn(Ox)/Zn(IMC) ratios of all three samples under formic acid decomposition conditions and after subsequent reduction. One can directly assess that $Zn_{52.1}Pd_{47.9}$ and $Zn_{49.8}Pd_{50.2}$ are significantly stronger oxidized than the $Zn_{42.0}Pd_{58.0}$ sample. At the most surface-sensitive photon energy (237 eV), more than 50 at.-% of the total Zn of Zn-rich ZnPd consist of oxidized species under reaction conditions, whereas at Pd-rich ZnPd less than 10 at.-% of oxidized Zn can be determined at the same photon energy. The difference between Zn-rich and equimolar ZnPd is not that pronounced but the general tendency reveals that Zn-rich ZnPd gets slightly stronger oxidized. Associated with the grade of oxidation the area of the O1s signal, which is localized at 530.4 eV,^[21] is changing, approving the alteration of the Zn3d region as oxidation phenomenon. The quantification of the Zn3d region after

subsequent reduction points out that the developing oxidized Zn species under formic acid conditions is only partially reversible – in line with the observations during the catalytic measurements in the reactor. Pd-rich and equimolar ZnPd nearly reach the same Zn(Ox)/Zn(IMC) ratios as before formic acid decomposition whereas especially at the most surface-sensitive measurements a slight increase of oxidized Zn species is present. However, in the case of Zn-rich the Zn(Ox)/Zn(IMC) ratio changes completely from 21 at.-% before to 32 at.-% after formic acid decomposition. These observations of changing oxidative behavior with changing chemical compositions and partially irreversible reaction state of Zn-rich ZnPd samples fits well with the inferences drawn out of the other characterization methods.

In contrast to the Zn signal, the Pd3d signal (recorded at BE between 335.7 eV for $Zn_{42.0}Pd_{58.0}$ and 336.2 eV for $Zn_{52.1}Pd_{47.9}$) was only slightly changing with different reaction conditions (Figure S5). The detected position range as well as the symmetric peak shape are characteristic for Pd in intermetallic ZnPd. Investigation of the C1s region revealed the appearance of a signal at the BE of 289.2 eV under reaction conditions which can be assigned to formate carbon^[22] (Figure S6). Both before and after formic acid decomposition only the characteristic carbon depositions from the *in situ* chamber could be detected. Therefore emerging of the formate signal together with an increase of the



oxidized Zn3d signal provides a strong indication for the presence of a zinc formate species during formic acid decomposition at 200 °C.

Figure 9. Depth-depending atomic Zn(Ox)/Zn(IMC) ratios of $Zn_{52.1}Pd_{47.9}$, $Zn_{49.8}Pd_{50.2}$ and $Zn_{42.0}Pd_{58.0}$ during formic acid decomposition (200 °C, 0.2 mbar formic acid) and after subsequent reduction in hydrogen (200 °C, 0.5 mbar) derived from XPS measurements.

FULL PAPER

To corroborate the XPS measurements, *operando* DTA/TG measurements on Zn-rich ZnPd under formic acid decomposition conditions at ambient pressures were conducted to investigate the supposed transition between zinc formate and zinc oxide (Figure 10). To achieve direct comparability, the ground $Zn_{51.9}Pd_{48.1}$ was pre-reduced in hydrogen inside the DTA/TG before formic acid decomposition. Formic acid decomposition was conducted by three consecutive heating/cooling cycles each with isothermal steps at the maximum (360 °C) and minimum (150 °C) temperature. After three cycles, the experiment was finished at 150 °C and the sample was cooled to room temperature while flowing He. During the first heating under formic acid decomposition conditions no sharp mass change can be observed. Only a minor mass increase, assumedly provoked by the surface formation of ZnO, is visible. During the first cooling the mass increases by 0.5 wt.-% with an onset temperature of 250 °C. The reversible character of the mass increase is becoming clear in the subsequent heating step where a mass loss, also occurring at an onset of 250 °C, is detected. The mass change during the heating and cooling steps is reproducible in the following cycles. In addition, the mass loss is not fully reversible. The observation perfectly fits to the picture of the previous investigations. If only formation of ZnO would take place, an irreversible mass gain would result under formic acid decomposition conditions. Thus, the increase in mass during the cooling steps beginning at 250 °C can be explained by the formation of a zinc formate species, which gets decomposed to zinc oxide above 250 °C. The irreversible mass gain is assigned to the formation of zinc oxide.

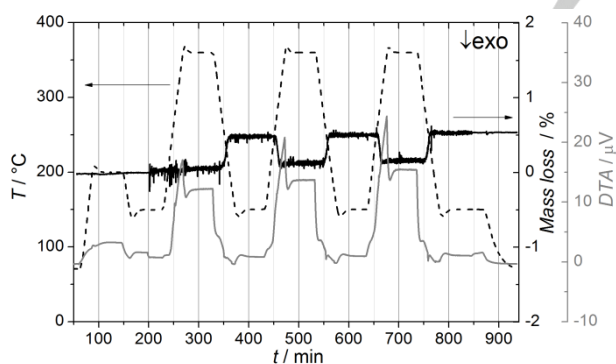


Figure 10. *Operando* DTA/TG measurement of $Zn_{51.9}Pd_{48.1}$ under formic acid decomposition conditions. The sample was pre-reduced in 10 vol.-% H_2/He (total gas flow 45 mL min^{-1}) at 200 °C for 1 h. After flushing for 30 min with pure He (45 mL min^{-1}) and simultaneously cooling down to 150 °C formic acid was initiated ($0.021 \text{ mL min}^{-1}$).

The DTA/TG was finished under formic acid decomposition conditions below 250 °C and the ZnPd sample was subsequently investigated by Raman spectroscopy (Figure 11). The most intense vibrational modes of formate ($\nu_s(\text{COO}^-)$: $1380, 1363 \text{ cm}^{-1}$; $2\nu_a(\text{COO}^-)$: 2795 cm^{-1} ; $\nu(\text{CH})$: $2910, 2895$; $\nu_a(\text{COO}^-)+\nu(\text{COO}^-)$: 2985 cm^{-1}) with corresponding relative intensities could be identified, thus strengthening the arguments above.^[23]

Characteristic modes for zinc oxide – appearing between 100 and 800 cm^{-1} – were not detectable.^[24]

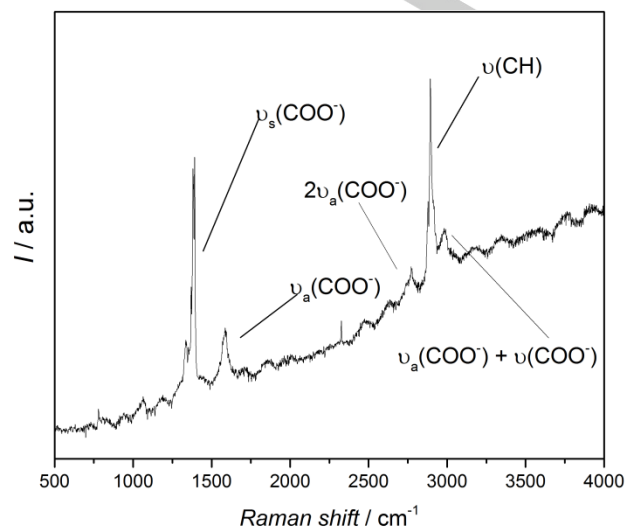


Figure 11. Raman spectrum of $Zn_{51.9}Pd_{48.1}$ after *operando* DTA/TG.

Correlations Between Formic Acid Decomposition and Methanol Steam Reforming

In general bulk ZnPd seems to exhibit similar changes during formic acid decomposition and methanol steam reforming concerning its oxidation behavior with composition. To retrieve more information, Table 1 lists the apparent activation energies of bulk ZnPd, ZnPd/ZnO and pure ZnO in formic acid decomposition and MSR collected from literature. The Arrhenius graphs of the apparent activation energies, determined in this study, are depicted in Figure S7-S10.

In formic acid decomposition two apparent activation energies were calculated for $Zn_{49.8}Pd_{50.2}$, $Zn_{51.9}Pd_{48.1}$ and ZnPd/ZnO because of the different behavior in the low ($< 240 \text{ °C}$) and high temperature ($> 240 \text{ °C}$) regime. By comparison of formic acid decomposition and MSR similar trends are realized with composition. In both reactions, the apparent activation energy decreases if intermetallic compound and oxide are simultaneously present. Correlation between both reaction mechanisms is thus conceivable. In MSR, the presence of ZnO is necessary to activate the water and thus achieve high CO_2 -selectivity. In contrast, formic acid decomposition also works on Pd-rich ZnPd compounds where formation of ZnO is suppressed. At Zn-rich ZnPd samples, the oxidation of Zn and adsorption/formation of formate seems to hinder the overall reaction rate. This is a hint that the dehydrogenation of the postulated formate intermediate takes place preferentially on the surface of the intermetallic compound and correlates with the observations of Lorenz et al. who investigated formic acid decomposition on $\beta\text{-Ga}_2\text{O}_3$ and intermetallic GaPd_2 .^[14] It is conspicuous that the apparent activation energies in Table 1 of

FULL PAPER

bulk and supported ZnPd determined in MSR are double as high as for formic acid decomposition on bulk ZnPd. This excludes the dehydrogenation of a formate species as rate determining step for the overall MSR reaction mechanism on ZnPd and ZnPd/ZnO, respectively, in difference to what was proposed earlier by quantum chemical calculations.^[8d]

Table 1. Apparent activation energies of bulk ZnPd, ZnPd/ZnO and ZnO in formic acid decomposition and MSR. Values without given reference were measured in the current study.

Sample	Apparent activation energy (kJ mol ⁻¹)	
	Formic acid decomposition	MSR
Zn _{42.0} Pd _{58.0} (150-240 °C)	53(2)	-
Zn _{49.8} Pd _{50.2} (150-210 °C / 240-330 °C)	32(3) / 47(3)	-
Zn _{49.8} Pd _{50.2} (300-500 °C)	-	120 ^[6]
Zn _{51.9} Pd _{48.1} (150-210 °C / 240-330 °C)	34(3) / 45(2)	-
ZnPd/ZnO (150-210 °C / 240-330 °C)	32(3) / 28(3)	-
ZnPd/ZnO (180-350 °C)	-	75 ^[5]
ZnO (170-210 °C)	105(8) ^[25]	-
ZnO (240-340 °C)	-	144 ^[9]

Conclusions

Single-phase samples of the intermetallic compound ZnPd with different chemical compositions (Zn_{51.9}Pd_{48.1}, Zn_{49.8}Pd_{50.2}, Zn_{42.0}Pd_{58.0}) and ZnO-supported ZnPd/ZnO were prepared. The samples were tested in formic acid decomposition and characterized by XRD, ICP-OES and SEM before and after reaction. All tested samples catalyze the decomposition of formic acid with high CO₂-selectivity up to 99.9%. Among the bulk ZnPd samples Zn_{42.0}Pd_{58.0} showed the highest activity. Unlike the Zn-rich samples, Zn_{42.0}Pd_{58.0} seemed to be more stable against surface oxidation under reaction conditions as has been proven by *operando* XPS measurements. XRD investigations after formic acid decomposition and *operando* DTA/TG indicate that Zn-rich ZnPd underwent a transformation caused by oxidative/reductive processes during formic acid, which effected the catalytic properties. ZnO-supported ZnPd showed the highest activity, as expected. Investigations of ZnPd/ZnO before and after reaction affirm a modification of the support caused by formation and decomposition of zinc formate. The apparent activation energies of bulk ZnPd and ZnPd/ZnO in MSR sample are two times higher than for formic acid decomposition. The experimental results imply that dehydrogenation of a formate intermediate does not

represent the rate limiting step in MSR on the intermetallic compound ZnPd.

Experimental Section

For the preparation of Zn_{100-x}Pd_x (x = 48.1-58.0) samples, Pd-foil (ChemPur, 99.9%, thickness: 0.25 mm, used in one piece) and zinc granules (ChemPur, 99.999%, diameter: 1-5 mm) were used. To obtain dense samples, the recently developed solid-vapor synthesis method was applied.^[26] Direct contact of Zn and Pd was avoided by means of a neck. The tube was placed in a furnace and the temperature was increased with 60 °C h⁻¹ to 500 °C. After 1 day of annealing, the temperature was raised to 900 °C with the same heating rate and held for 10 days. Finally, the ampoule was quenched in water. No interaction of the reactants with the quartz glass ampoule was observed. ZnO-supported ZnPd particles were prepared using 4.99911 g ZnO (AlfaAesar, 99.99% metals basis) and 1.52558 g Pd(NO₃)₂ · xH₂O (AlfaAesar, 99.9% metals basis) following a standard incipient wetness impregnation based on the synthesis route of Iwasa et al.^[4] The single-phase nature of the intermetallic bulk samples was verified by powder X-ray diffraction (Huber image plate G670, Cu Kα₁, λ = 1.54056 Å, quartz monochromator, 3° < 2θ < 100°). Unit cell parameters were determined using the program WinCSD^[27] with LaB₆ as internal standard (a = 4.15692 Å). Elemental analysis was conducted by ICP-OES (Vista RL, Varian) by dissolving the samples in aqua regia. The elemental composition was analyzed in triplicate after matrix matched calibration.

Catalytic measurements were carried out in a plug-flow reactor system (Microactivity Reference, PID Eng&Tech). For the catalytic tests the Zn_{100-x}Pd_x samples were ground in air, sieved to a particle size between 20 and 32 μm and mixed with 200 mg of graphite (ChemPur, >99.9%) to dilute the catalyst bed. For better comparison the herein described catalytic tests of bulk ZnPd were all conducted with a sample mass of 50 mg. The used graphite was tested before to be inactive in formic acid decomposition as well as the water gas shift reaction. ZnPd/ZnO was also mixed with 200 mg graphite before catalytic tests. Catalysts were placed inside a silica-coated stainless steel tube (inner diameter 7.9 mm) which was mounted inside a hotbox to prevent condensation of liquids. All samples were pre-treated directly before formic acid decomposition to reach a defined starting point. The ZnPd bulk samples were reduced in 100 vol.-% H₂ (Praxair, 99.999%, 3 ml min⁻¹) at 200 °C for 1 h identical to the chosen pre-treatment conditions of Friedrich et al.^[6] The supported material was calcined at 500 °C in synthetic air (Praxair, 99.999%, 40 ml min⁻¹) for 3 h and subsequently reduced in 5 vol.-% H₂ (total gas flow 40 ml min⁻¹) at 500 °C for 2 h. Catalytic tests consisted of two heating sessions and an intermediate cooling session. The samples were heated/cooled in 30 °C steps with 1 h of holding time at every step to allow for equilibration before taking data from which the apparent activation energy was determined. The reactive feed consisted of 0.021 ml min⁻¹ formic acid (Sigma Aldrich, ≥ 98%) which was evaporated before being mixed with 41 ml min⁻¹ N₂ (Praxair, 99.999%) and 4 ml min⁻¹ He (Praxair, 99.999%). Helium was applied as internal standard to calibrate the gas volumes while N₂ was used as carrier gas. For determination of the gas composition in the product stream a gas chromatograph (Varian Micro GC CP4900) was used, allowing quantitative determination of CO (column: Al₂O₃/KCl, carrier gas: He, sensitivity down to 20 ppm), CO₂ (column: Pora Plot U, carrier gas: He) and H₂ (column: MS 5A, carrier gas: Ar from Messer with 99.999% purity) every four minutes. To determine conversion and selectivity all GCs per isothermal step were averaged. Unconverted formic acid, as well as produced water were not determined by GC because they were separated by a cooling trap and a subsequent Nafion® membrane. Remaining traces of liquid in the product gas stream were finally removed by cooling the

FULL PAPER

product stream to -60 °C. The conversion of formic acid is calculated as $C = (\text{CO}_{x,\text{out}}/\text{CO}_{x,\text{max}}) \times 100$, wherein $\text{CO}_{x,\text{out}}$ is the summed concentration of CO and CO₂ in the product gas and $\text{CO}_{x,\text{max}}$ is the concentration of carbon oxides that can be generated if all formic acid is converted according to the reaction equations $\text{HCOOH} \rightarrow \text{H}_2\text{O} + \text{CO}$ and $\text{HCOOH} \rightarrow \text{H}_2 + \text{CO}_2$, respectively. The CO₂-selectivity $S(\text{CO}_2)$ is calculated as $\text{CO}_{2,\text{out}}/\text{CO}_{x,\text{out}} \times 100$, wherein $\text{CO}_{2,\text{out}}$ is the concentration of CO₂ in the product gas. The activity is defined as $A = \text{CO}_{x,\text{out}}/(n_{\text{Pd}} \times t)$, wherein n_{Pd} is the molar amount of palladium used and t is time.

Scanning electron microscopy (SEM, FEI Quanta 200F, cold FEG) was conducted to investigate the morphology of the supported sample before and after catalytic measurement. Prior to SEM imaging, graphite – which was used as filling material during formic acid decomposition – was mostly separated by sieving. Samples were mounted on Al-holders using conducting carbon tape prior to analysis.

Operando DTA/TG measurements (Netzsch, STA 449 F3 Jupiter) of Zn_{51.9}Pd_{48.1} under formic acid decomposition conditions were conducted to investigate changes of the catalyst sample during heating and cooling cycles. Similar to catalytic investigations, bulk ZnPd was ground in air to powder. Prior to formic acid decomposition the sample was reduced in 10 vol.-% H₂/He (total gas flow 45 mL min⁻¹) at 200 °C for 1 h. After flushing for 30 min with pure He (45 mL min⁻¹) and simultaneously cooling down to 150 °C formic acid was introduced (0.021 mL min⁻¹). Three heating/cooling cycles, each with a rate of 5 K min⁻¹ and one hour isothermal steps at the minimum (150 °C) and maximum (360 °C) temperature were conducted before cooling down to room temperature. The measurement was background corrected to eliminate any non-sample effects.

Raman spectra of Zn_{52.1}Pd_{48.1} after *operando* DTA/TG were measured with a Horiba Jobin-Yvon Labram O10 spectrometer at ambient conditions in backscattering geometry. For excitation the green Ar ion laser line (488 nm) with a power of 30 mW at the sample was used. Acquisition time per spectrum ranged from 100 to 2000 s. The sample was measured at different positions to ensure characteristic spectra.

In situ X-ray photoelectron spectroscopy (*in situ* XPS) was conducted at the ISSS-PGM beamline, Helmholtz Zentrum Berlin für Materialien und Energie – Electron storage ring BESSY II. The setup is described in detail elsewhere^[28] Bulk ZnPd samples with different chemical composition were prepared by the foil method as already described. To ease the mounting of the samples on the sapphire holder the Pd-foils were punched into round pieces with a diameter of 8 mm prior to synthesis. Pre-reduction in hydrogen was performed *in situ* at 0.5 mbar hydrogen pressure and 200 °C while measuring the Zn3d signal to monitor the surface reduction. After reaching a stable state, the samples were cooled to ambient temperature and the core levels of Pd3d, Pd3p, Zn3d, O1s and C1s were recorded at pressures of 10⁻⁸ mbar. To achieve depth profiling of the samples, core levels were measured at five different kinetic energies (232, 382, 532, 682 and 832 eV). Experiments under *operando* formic acid decomposition conditions were conducted at 0.2 mbar formic acid and 200 °C. Formation of reaction products as an indication of catalytic activity during the measurements was detected by a mass spectrometer (Pfeiffer Prisma). After formic acid decomposition, the samples were reduced and measured once again to check the reversibility in the changes to the near-surface region. The signals were energy corrected by the fermi edge before qualitative and quantitative evaluation using the software Casa XPS.^[29] Prior to the fitting of the signal areas the background was subtracted by applying the Shirley-type of background. During the fitting of the signals the ratio between the doublet signals (Pd3d_{5/2}:Pd3d_{3/2} and Zn3d_{5/2}:Zn3d_{3/2} = 3:2, Pd3p_{3/2}:Pd3p_{1/2} = 2:1) as well as the distance between the doublet signals ($\Delta\text{Pd3d}_{5/2}/\text{Pd3d}_{3/2} = 5.26$ eV, $\Delta\text{Zn3d}_{5/2}/\text{Zn3d}_{3/2} = 0.4$ eV, $\Delta\text{Pd3p}_{3/2}/\text{Pd3p}_{1/2} = 22.6$ eV) was constrained.

Fitted areas were corrected considering ring current, photon flux and the respective cross sections.^[30] The calculation of information depths relies on the inelastic mean free path (IMFP) through the NIST Standard Reference Database 71^[31] based on the work of Tanuma et al.^[32] As an approximation the IMFP of elemental Pd was used. The information depth is defined as three times the IMFP, i.e. 95% of the excited electrons originate from the respective depth.^[33]

Acknowledgements

The authors thank J. Grin for his unfathomable support especially during the move from the MPI CPFS in Dresden to the Technical University Chemnitz. We acknowledge the Helmholtz Zentrum Berlin für Materialien und Energie – Electron storage ring BESSY II – for providing beamtime at the ISSS beamline (Project No. 14201526ST) and J. Velasco-Vélez, T. Keilhauer, M. Meier and R. Blume for supporting the XPS measurements. The authors also thank W. Reschetilowski for valuable discussion.

Keywords: Formic acid decomposition • Intermetallic compound • Methanol steam reforming • ZnPd

- [1] Y. Brunet, *Energy Storage*, Wiley-VCH, Weinheim, **2013**.
- [2] P. Gruss, F. Schüth, *Die Zukunft der Energie*, C. H. Beck, München, **2008**.
- [3] G. Bender, M. Angelo, K. Bethune, R. Rocheleau, *J. Power Sources* **2013**, *228*, 159-169.
- [4] N. Iwasa, S. Masuda, N. Ogawa, N. Takezawa, *Appl. Catal.*, **A 1995**, *125*, 145-157.
- [5] M. Friedrich, S. Penner, M. Heggen, M. Armbrüster, *Angew. Chem. Int. Ed.* **2013**, *52*, 4389-4392; *Angew. Chem.* **2013**, *125*, 4485.
- [6] M. Friedrich, D. Teschner, A. Knop-Gericke, M. Armbrüster, *J. Catal.* **2012**, *285*, 41-47.
- [7] T. H. Chiang, H. Ipser, Y. A. Chang, *Z. Metallkd.*, **1977**, *68*, 141-147.
- [8] a) Z. X. Chen, K. M. Neyman, K. H. Lim, N. Rösch, *Langmuir* **2004**, *20*, 8068-8077; b) K. H. Lim, Z.-X. Chen, K. M. Neyman, N. Rösch, *J. Phys. Chem. B* **2006**, *110*, 14890-14897; c) Z. X. Chen, K. H. Lim, K. M. Neyman, N. Rösch, *J. Phys. Chem. B* **2005**, *109*, 4568-4574; d) S. Lin, D. Xie, H. Guo, *J. Phys. Chem. C* **2011**, *115*, 20583-20589; e) S. Lin, D. Xie, H. Guo, *J. Mol. Catal. A: Chem.* **2012**, *356*, 165-170; f) G. K. Smith, S. Lin, W. Lai, A. Datye, D. Xie, H. Guo, *Surf. Sci.* **2011**, *605*, 750-759.
- [9] H. Lorenz, M. Friedrich, M. Armbrüster, B. Klötzer, S. Penner, *J. Catal.* **2013**, *297*, 151-154.
- [10] M. Armbrüster, M. Behrens, K. Föttinger, M. Friedrich, E. Gaudry, S. K. Matam, H. R. Sharma, *Cat. Rev. - Sci. Eng.* **2013**, *55*, 289-367.
- [11] a) E. S. Ranganathan, S. K. Bej, L. T. Thompson, *Appl. Catal.*, **A 2005**, *289*, 153-162; b) A. Haghofer, D. Ferri, K. Föttinger, G. Rupprechter, *ACS Catal.* **2012**, *2*, 2305-2315.
- [12] G. C. Bond, *Catalysis by Metals*, Academic Press, **1962**.
- [13] a) G. Rienäcker, *Z. Elektrochem.* **1934**, *40*, 487-488; b) G. Rienäcker, *Z. Anorg. Allg. Chem.* **1936**, *227*, 353-375.
- [14] H. Lorenz, R. Thalinger, E.-M. Köck, M. Kogler, L. Mayr, D. Schmidmair, T. Bielz, K. Pfaller, B. Klötzer, S. Penner, *Appl. Catal.*, **A 2013**, *453*, 34-44.
- [15] E. Jerero, J. M. Vohs, *Catal. Lett.* **2009**, *130*, 271-277.
- [16] S. Penner, M. Armbrüster, *ChemCatChem* **2015**, *7*, 374-392.
- [17] Y. Noto, K. Fukuda, T. Onishi, K. Tamaru, *Trans. Faraday Soc.* **1967**, *63*, 3081-3087.
- [18] a) K. A. Hofmann, K. Schumpelt, *Ber. Dtsch. Chem. Ges.* **1916**, *49*, 303-317; b) Dollimore, D. K. H. Tonge, *J. Inorg. Nucl. Chem.* **1967**, *29*, 621-627.

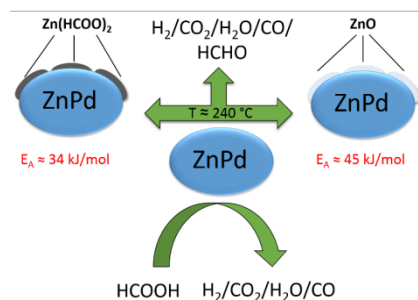
FULL PAPER

- [19] A. M. Bahmanpour, A. Hoadley, A. Tanksale, *Green Chem.* **2015**, *17*, 3500-3507.
- [20] N. Iwasa, H. Suzuki, M. Terashita, M. Arai, N. Takezawa, *Catal. Lett.* **2004**, *96*, 75-78.
- [21] E. Agostinelli, C. Battistoni, D. Fiorani, G. Matogno, *J. Phys. Chem. Solids* **1989**, *50*, 269-272.
- [22] S. Yumitori, *J. Mater. Sci.* **2000**, *35*, 139-146.
- [23] J. Hedberg, S. Baldelli, C. Leygraf, *J. Electrochem. Soc.* **2010**, *157*, C363-C373.
- [24] N. Panwar, J. Liriano, R. S. Katiyar, *J. Alloys Compd.* **2011**, *509*, 1222-1225.
- [25] T. Kondo, T. Ogawa, K. Kishi, K. Hirota, *Z. Phys. Chem.* **1969**, *67*, 284-290.
- [26] D. C. A. Ivarsson, U. Burkhardt, K. Richter, R. Kriegel, L. Rößner, M. Neumann, M. Armbrüster, *J. Alloys Compd.* **2018**, accepted manuscript.
- [27] L. G. Akselrud, Y. P. Zavalii, Y. N. Grin, V. K. Pecharski, B. Baumgartner, E. Wölfel, *Mater. Sci. Forum* **1993**, *133-136*, 335-342.
- [28] M. Salmeron, R. Schlögl, *Surf. Sci. Rep.* **2008**, *63*, 169-199.
- [29] Casa XPS (Version 2.3.16), **2010**.
- [30] J. J. Yeh, I. Lindau, *At. Data Nucl. Data Tables* **1985**, *32*, 1-155.
- [31] NIST Electron Inelastic-Mean-Free-Path Database, **2010**.
- [32] S. Tanuma, C. J. Powell, D. R. Penn, *Surf. Interface Anal.* **1991**, *17*, 911-926.
- [33] J. C. Vickerman, I. S. Gilmore, *Surface Analysis – The Principle Techniques, Vol. 2*, Wiley, Chichester, **2009**.

FULL PAPER

FULL PAPER

The reaction mechanism of methanol steam reforming (MSR) on ZnPd was investigated by use of catalytic formic acid decomposition as model reaction. On the basis of determined apparent activation energies we conclude that dehydrogenation of a formate intermediate does not represent the rate limiting step.



René Kriegel, Dennis C. A. Ivarsson, and Marc Armbrüster*

Page No. – Page No.

Formic Acid Decomposition over ZnPd – Implications for Methanol Steam Reforming